Journal of Building Engineering 49 (2022) 104019

Contents lists available at ScienceDirect

Journal of Building Engineering

journal homepage: www.elsevier.com/locate/jobe

A novel macroelement for seismic analysis of unreinforced masonry buildings based on MVLEM in OpenSees

Amirhosein Shabani [*], Mahdi Kioumarsi [**]

Department of Civil Engineering and Energy Technology, Oslo Metropolitan University, Pilestredet 35, 0166, Oslo, Norway

ARTICLE INFO

Keywords:
Seismic analysis
Unreinforced masonry buildings
Equivalent frame method
Macroelement model
MVLEM element

ABSTRACT

Unreinforced masonry (URM) buildings are susceptible to extraordinary actions such as earthquakes compared to steel or reinforced concrete buildings. Various methods have been developed for the computational analysis of URM buildings in the last few decades. The equivalent frame method (EFM) is one of the numerical modeling approaches widely used for the nonlinear analyses of URM buildings. Different macroelements in the context of the EFM have been proposed. However, there is still a need for an efficient modeling approach in the computational effort that can predict the real behavior of URM structural components with sufficient agreement and available in opensource structural analyses software packages. For this purpose, a new macroelement based on the multiple vertical line element method (MVLEM) element has been developed in this study. The MVLEM is available in the OpenSees software platform comprising vertical uniaxial macro-fibers and a shear spring as an efficient macroelement for nonlinear analysis of flexure-dominated reinforced concrete walls. The novel macroelement, double modified MVLEM (DM-MVELM) element has been proposed consisting of two modified MVLEM elements tied with a nonlinear shear spring at the middle with a trilinear backbone behavior. DM-MVLEM can capture the axial-flexural interaction with lower computational effort than finite element models and fiber beam-column elements. The DM-MVLEM has been validated against the test results at the structural components level and a full-scale perforated URM wall. Unified method (UM) and composite spring method (CSM) are two existing EFMs that are presented in this study. A study is performed by comparing the seismic behavior of the perforated URM walls modeled using the UM, CSM, and DM-MVLEM modeling strategies. Results show that the DM-MVLEM can predict the damage patterns, and nonlinear behavior of spandrels can be simulated that was usually modeled with linear behavior in EFMs.

* Corresponding author.
** Corresponding author.
E-mail addresses: amirhose@oslomet.no (A. Shabani), mahdik@oslomet.no (M. Kioumarsi).

https://doi.org/10.1016/j.jobe.2022.104019
Received 4 October 2021; Received in revised form 5 January 2022; Accepted 7 January 2022
Available online 12 January 2022

Nomenclature

A	Cross-sectional area of URM components
b	Width of a Pier
b_{eff}	Effective interlocking length of URM units
b_h	Thickness of a brick plus a mortar joint
c	Location of center of rotation of the MVELM element
E	Elastic modulus of masonry
f_c	Compressive strength of masonry
f_{td}	Diagonal tensile strength of masonry
f_{teq}	Equivalent tensile resistance of a spandrel segment due to interlocking
f_{v0}	Shear strength of masonry at zero compressive stress (cohesion)
G	Shear modulus of masonry
h	Height of a pier
h_{sp}	Depth of a spandrel neglecting the lintel
h_t	Total height of a URM wall
H_{eff}	Height of piers considering cantilever idealization of spandrels
I_g	Inertia moment of a pier
I_w	Inertia moment of a whole URM wall
K_0	Initial in-plane stiffness of a URM wall
K_{Es}	Shear stiffness of a URM wall
K_{Eu}	Initial in-plane stiffness of a URM pier segment with definite boundary conditions
L	Length of a pier
t	Thickness of URM components
V_D	Maximum shear strength of a URM segment based on the diagonal cracking failure mode
V_I	Interlocking shear strength of bed joint of spandrels
V_m	Maximum shear strength of a URM segment
V_R	Maximum shear strength of a URM segment based on the rocking failure mode
V_S	Maximum shear strength of a URM segment based on the shear sliding failure mode
α_0	Zero-moment coefficient
α_y	Fraction of the yielding shear strength on the maximum shear strength
β	Stiffness degradation factor due to ductility
ζ	Shear stress distribution coefficient at the center of a pier
η	Ratio between the secant stiffness corresponding to V_m and K_0
η_{soft}	Softening stiffness coefficient
η_a	Coefficient for allocating the vertical compression
λ	Revision coefficient accounting for the compression ratio and aspect ratio for calculating V_m
σ_0	Vertical compression stress
σ_p	Vertical compressive stress in the adjacent piers of a spandrel
μ	Friction coefficient

1. Introduction

Unreinforced masonry (URM) construction system composed of brick units and mortar is a typology that is prevalent in high seismicity zones, i.e., southern European countries and the Middle East [1,2]. Experience from the past earthquakes has revealed that the URM construction system is vulnerable due to the brittle characteristic of the masonry, weak connections between the vertical and horizontal components, and susceptible connection between floor system and URM walls that leads to a considerable increase in losses for authorities [3–5]. Although studies on the seismic design and analyses of reinforced concrete and steel structures have gained more attention in recent years, studies on the seismic vulnerability assessment of URM structures have increased dramatically [3,6,7].

Masonry and timber are considered as the oldest construction material, abundantly found in historic areas [8,9]. Due to the brittle behavior of masonry as a low tensile strength material, existing URM buildings show nonlinear behavior even at the early stage of seismic loading; therefore, incremental iterative nonlinear analyses is a crucial part of an accurate seismic vulnerability assessment methodology [10,11]. Nonlinear static or pushover analysis (POA) is widely used for the seismic vulnerability assessment of URM buildings, and different assessment methodologies such as the N2 method [12] based on the POA results have been developed [13–15]. The POA results can be highly dependent on the load pattern applied on buildings [16]. Nonlinear time history analysis (NTHA) can be considered as the most robust analysis method for seismic vulnerability assessment [17,18]. Earthquake records specification, i.e., their duration, the sequence of peaks, and the frequency content are considered in NTHA, but are neglected in the monotonic POA procedure [13,19]. Nevertheless, the NTHA has been utilized sparingly for the seismic vulnerability assessment of buildings due to the

considerable computational efforts required [20,21].

Limit analysis-based solutions have also been utilized to calculate the collapse multipliers and the collapse mechanisms [1]. Compared to the incremental iterative analyses approaches, load-bearing behavior, including maximum displacement or post-peak response, cannot be derived using the limit analysis-based solutions [22]. Limit analysis-based methods by modeling structures using rigid blocks were utilized for collapse analysis of masonry towers [23,24], arches [25,26], and buildings [27–30].

Understanding the probable failure modes of URM walls is a crucial part of nonlinear modeling. Failure modes of URM walls subjected to combined vertical and in-plane loadings are dependent on the different properties such as wall aspect ratio, mechanical properties of masonry, and boundary conditions [31–33]. Fig. 1 shows three types of failure modes of URM walls. In the shear sliding failure mode (see Fig. 1 (a)), sliding along a single mortar bed-joint line or in a stepwise fashion along bed-joints and head-joints occurs that usually can be detected in walls with a low aspect ratio (squat walls). The diagonal cracking failure mode involves both masonry units and mortar joints, with the formation of a diagonal crack starting from the middle of the wall and propagating toward the corners, as shown in Fig. 1 (b). The rocking failure mode produces tensile or crushing cracks or both at the corner of the wall, as depicted in Fig. 1 (c), which most frequently occurs in walls with high aspect ratios (slender walls) [19,21,31].

Due to the composite and non-homogenous nature of masonry, modeling URM buildings poses a challenge. Modeling procedures that are associated with the incremental-iterative analyses approaches can be divided into three main groups: 1) discrete element model (DEM) 2) continuum homogenous model (CHM), and 3) equivalent frame model (EFM) [1,14]. In DEMs, the actual texture of masonry is identified by modeling mortar joints and masonry units [34,35]. In CHMs, no distinction between individual masonry units and mortar is considered. Less computational effort and fewer input data, as well as an easy modeling procedure, are the main advantages of CHMs over DEMs [14]. CHMs are widely used for nonlinear analysis of full-scale cultural heritage assets with complex architecture where out-of-plane failure mechanics may be critical [4,36,37].

EFMs are widely used for the global seismic assessment of existing URM buildings in engineering practice [10]. In EFMs, a perforated wall is discretized to vertical (piers) and horizontal (spandrel) components that are connected with rigid zones [1]. Although both in-plane and out-of-plane collapse mechanisms are considered in other mentioned models, in the EFMs, the out-of-plane mechanisms have been usually neglected [10], and this approach is consistent with FEMA 356 guideline [38]. Moreover, well-known EFM software packages (e.g., 3Muri [39]) neglect the out-of-plane contribution of the walls, but investigate the local collapse mechanisms through a separate analysis by neglecting the interactions between the global and local seismic responses [29,40].

Fig. 2 shows a schematic overview of the two incremental iterative analysis methods versus related modeling approaches utilized for the seismic vulnerability assessment of URM buildings by emphasizing the computational efforts level. Fig. 2 indicates that the NTHA of DEMs is considered to be the least common methodology for the seismic vulnerability assessment of URM buildings, but the POA of EFMs is widely used nowadays by practitioners due to its simplicity and efficiency.

Keeping the simplicity of modeling and lowering the uncertainties, stochastic NTHA of the EFMs will be an alternative to the simplified analytical methods for seismic vulnerability assessment of URM buildings at a large scale or an efficient tool for analysts. This study focuses on the NTHA of EFMs as illustrated in the black box in Fig. 2.

The first developments of EFM originated from the POR method [41]. A simple elasto-plastic behavior was considered for beam nonlinearity with assuming rigid spandrel and nodal zones. This approach was then developed by implementing shear and rocking hinges for piers and spandrels in SAP 2000 software package [19]. However, due to the high level of computational efforts for the NTHA, the rocking hinges at the two ends of the piers and shear springs in the middle of the spandrels were omitted [19]. In order to investigate the axial-shear (N-V) interaction, a method implementing two rotational plastic hinges at two ends of beam elements was developed in SAP 2000 [21]. This method was then simplified by neglecting the N-V interaction in the pier hinges and considering linear spandrels [42]. A two-node macroelement consists of three parts: a central body, where only shear deformations are possible, and two interfaces, where the external degrees of freedom has been developed [43]. This macroelement is calibrated to account for the accurate enough cyclic behavior of both flexural and shear failure mechanisms and implemented in the 3Muri software package [39]. This macroelement is then modified to tackle the limitations i.e., the inability to capture at the same time both axial and flexural stiffnesses of the element and neglect of the N-V interaction during the analysis procedure [44,45]. By developing fiber beam elements considering a spread plasticity model, different methods were proposed to consider the axial-flexural (N-M) interaction in structural

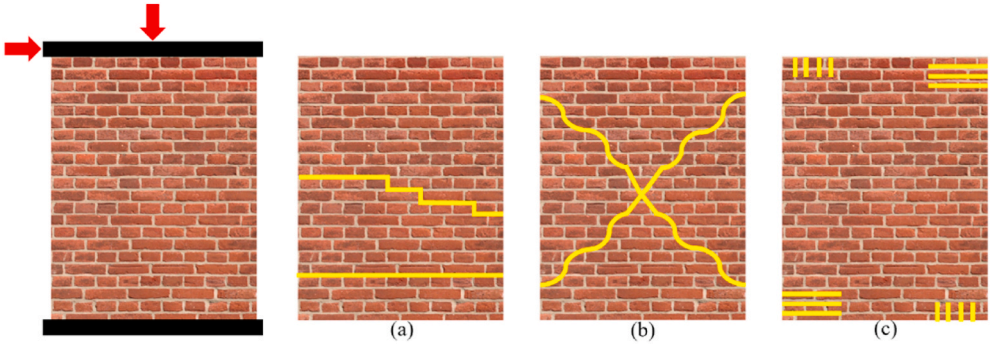

Fig. 1. Crack patterns of a URM wall subjected to axial and lateral loadings for the shear sliding (a) diagonal cracking (b), and rocking (c) failure modes [21].

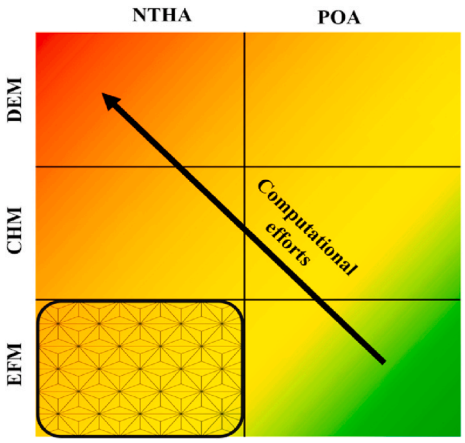

Fig. 2. Schematic overview of different incremental iterative analysis methods as a function of the relevant numerical modeling methods and corresponding computational efforts.

components [46,47]. The nonlinear response of the fibers is simulated by the mono-axial constitutive law of masonry, and a nonlinear shear spring has been implemented in the middle of the element to represent shear failure behavior [47].

Using spring elements for modeling both perforated and unperforated URM walls is a simplified approach that has been employed in the unified method (UM) [48]. In the UM, a URM wall is characterized by a nonlinear shear spring per story [48]. However, by using the composite spring method (CSM) as a more detailed method than the UM, nonlinear shear springs are assigned to each structural component [49]. A nonlinear shear spring is characterized by a definite backbone curve and hysterics rules dependent on the possible failure mode of the structural components [49]. In order to capture all the failure modes, including the combined flexural and shear failure modes, in piers and spandrels and incorporate an exact enough hysterics model for performing the NTHA, a spring-based macroelement was developed and validated against the experimental tests [50]. The macroelement comprises two rotational

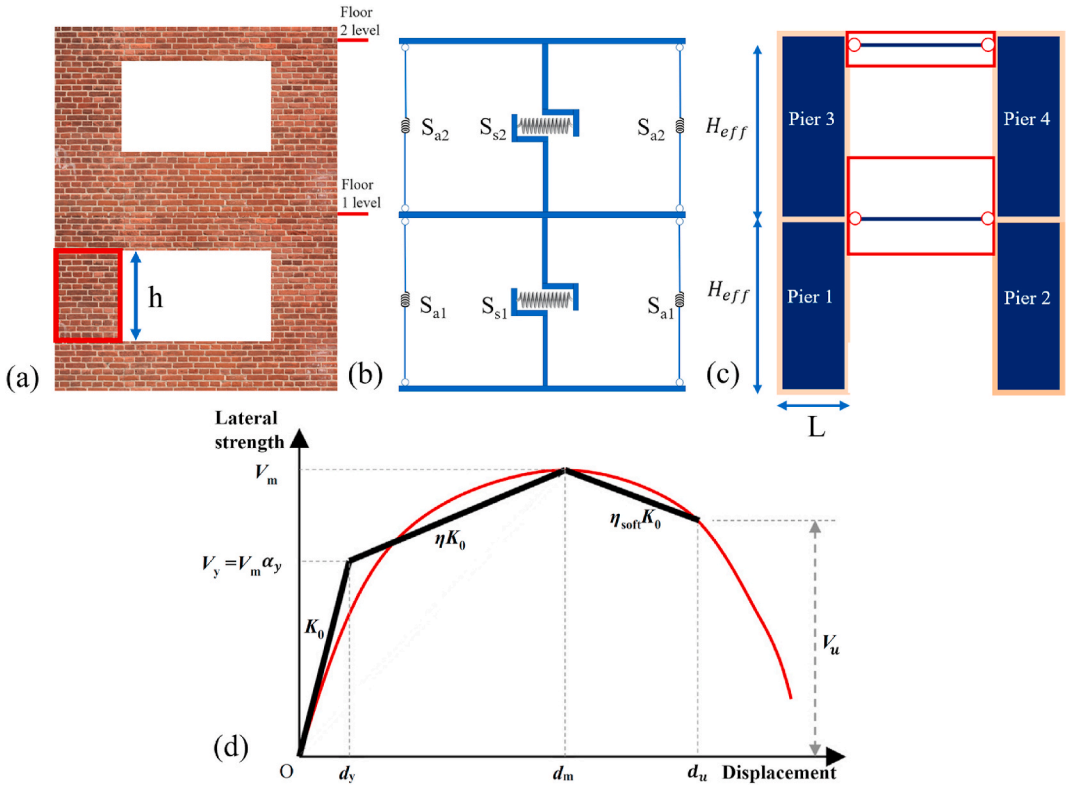

Fig. 3. (a) A perforated URM wall, (b) a schematic view of the wall modeled using the UM and configuration of axial and shear springs, (c) the discretization of the wall to piers to derive the maximum shear strength of each story, and (d) the backbone curve of the nonlinear shear spring.

springs at the two ends of the structural components to capture the flexural behavior and a shear spring to reflect the shear failure [50].

In this study, multiple-vertical-line-element-model (MVLEM), a macroelement model developed for modeling the flexure dominated reinforced concrete (RC) shear walls, is utilized to innovate a macroelement for the seismic analysis of URM buildings. An MVLEM element comprises a set of uniaxial nonlinear fiber elements connecting upper and lower rigid beam elements and a nonlinear shear spring which is located at a specific height [51,52]. Simple formulation, numerical stability, the efficiency of computational effort, the ability to capture important features such as shifting of the neutral axis, and the effect of a fluctuating axial force on strength and stiffness are the main characteristics of the MVLEM element that is available in OpenSees framework [51,53]. The MVLEM element cannot reflect the N-V interaction. To tackle this limitation, this element was improved by incorporating macro-fiber elements that allow coupling of N-M and shear responses at the model element level [54–56].

The new macroelement called DM-MVLEM consists of two modified MVLEMs that are tied together with a nonlinear shear spring. DM-MVLEM validated against the experimental tests on two piers, one spandrel, and a full-scale perforated URM wall. Furthermore, UM and CSM are selected and among the existing EFMs and modified to perform a comparative study. The methods' performance for capturing the nonlinear behavior and damage pattern prediction of URM buildings has been investigated by performing pushover and incremental dynamic analyses.

2. Overview of existing macroelements

In this section, the procedure of two existing macroelements for nonlinear dynamic analysis of URM buildings is presented. Firstly, the UM procedure is reviewed as the simplest method in this study, and some modifications have been suggested. Moreover, as the second method, the CSM is developed based on the shear constitutive law of URM piers presented in the UM with manipulation of the hysteresis rules validated against the test results.

2.1. Unified method (UM)

The UM was proposed as a simplified method for the seismic analysis of confined and unconfined masonry structures with and without openings [48]. In this approach, a URM wall of a story is modeled with a unique macroelement that consists of two vertical linear springs at two corners of a wall to transfer the axial loads and a nonlinear shear spring modeled at the middle of the wall to represent the nonlinear shear behavior of the wall as it is illustrated in Fig. 3 (b). The two axial springs (S_a) are located at two sides of a wall with the stiffness of $\frac{EA}{2h}$, where E is the elasticity modulus, A is the cross-section area, and h is the height of the wall. As illustrated in Fig. 3 (d), the shear spring (S_s) consists of a nonlinear material with the backbone curve to capture the shear failure behavior of the wall in such a way that two other degrees of freedom are free [48].

For the perforated URM walls, a conservative approach by assuming uncoupled piers is considered for deriving the maximum shear strength. This corresponds to the cantilever idealization that null shear strength is considered for the spandrels [39], and the term H_{eff} is the height of the vertical component as illustrated in Fig. 3 (c). Therefore, as shown in Fig. 3 (c), the total height of each floor is utilized for all the piers of each floor, and the total shear strength is calculated as the sum of the shear strength of the piers. As investigated in Ref. [48], the maximum shear strength can be computed for the piers based on:

$$V_m = 2.15\lambda^{0.256}\left[\frac{1}{1.2}\sqrt{1+\eta_a\frac{\sigma_0}{f_{v0}}}+\mu(1-\eta_a)\frac{\sigma_0}{f_{v0}}\right]f_{v0}A \tag{1}$$

where σ_0 is the compression stress, f_{v0} is the shear strength of the masonry at zero compressive stress, a value of 0.6 is suggested for the term η_a which is the coefficient for allocating the vertical compression, μ which is the friction coefficient is suggested to be 0.4 [48], A is the cross section of each pier segment, and λ factor is calculated as:

$$\lambda = \begin{cases} \frac{\sigma_0}{f_c}e^{-\frac{H_{eff}}{L}} \; when \; 0 < \frac{H_{eff}}{L} \le 0.675 \\ \frac{\sigma_0}{f_c}e^{-1.55\frac{H_{eff}}{L}} \; when \; \frac{H_{eff}}{L} > 0.675 \end{cases} \tag{2}$$

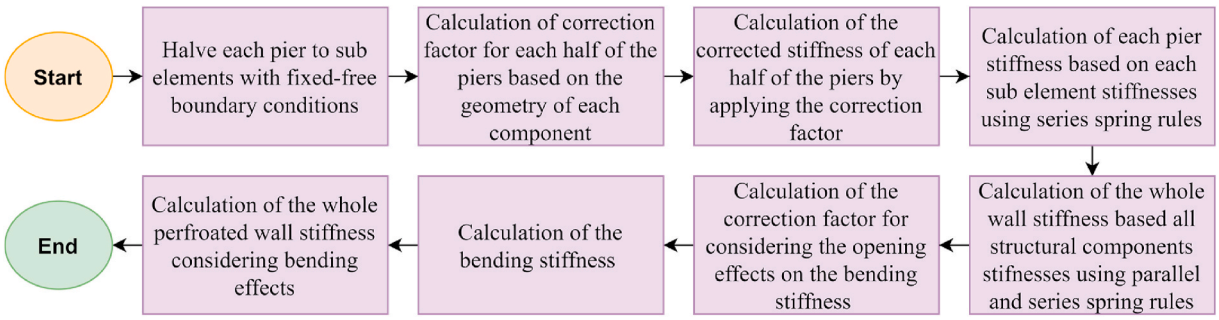

Fig. 4. Workflow of EHM for calculating the initial in-plane stiffness of perforated URM walls.

where f_c is the compressive strength of masonry, and L is the length of the piers as illustrated in Fig. 3 (c).

Initial in-plane stiffness is a crucial parameter for defining the backbone curve that can be calculated as follows for unperforated URM walls with fixed-fixed and fixed-free boundary conditions, respectively:

$$K_{Eu} = \frac{1}{\frac{h^3}{12EI_g} + \frac{1.2h}{GA}} \tag{3}$$

$$K_{Eu} = \frac{1}{\frac{h^3}{3EI_g} + \frac{1.2h}{GA}} \tag{4}$$

where h is the height of a pier as illustrated in Fig. 3 (a), G is shear modulus, and I_g is the moment of inertia of the wall cross section. However, due to flexible boundary conditions of piers in perforated URM walls, utilizing Equation (3) will overestimate the initial in-plane stiffness. In order to calculate the initial stiffness of perforated walls, effective height method (EHM) is considered a simplified analytical method clarified in Refs. [57,58]. A comparative study was done in Ref. [59], and it is investigated that the EHM can be an exact enough method validated against the FEM results compared to the analytical method presented in the UM literature [48]. The workflow of the EHM to derive the initial in-plane stiffness (K_0) of a perforated URM wall is depicted in Fig. 4, and more details are in Refs. [58,59].

After deriving V_m, and K_0, as illustrated in Fig. 3 (d) trilinear backbone curve can be derived based on α_y for calculating the yielding strength, η which is the ratio between the secant stiffness corresponding to V_m and K_0, and η_{soft} is the softening stiffness coefficient [48]. For simulating the hysteresis rules, the Hysteretic material in the OpenSees framework can be utilized, and details about the effects of each parameter are presented in Ref. [53]. The pinching factors for strain and stress during reloading and the stiffness degradation factor are presented in Table 1 in accordance with [48], and a value of 0.05 is considered for the damage due to the energy factor.

2.2. Composite spring method (CSM)

The well-known EFM characterized by assigning nonlinear shear springs to the middle of linear beam-column elements for simulating the nonlinear behavior of piers is presented in Refs. [19,49,60]. In the CSM, a perforated URM wall is discretized to piers and spandrels, and a nonlinear spring is assigned to each pier. For discretizing the structural components, the method proposed by Dolce [61] was utilized. Based on this method, the spandrels and piers were divided and connected with rigid elements such that the length of the spandrels equals the length of the openings, and the effective height of the piers has been derived by the intersection between the vertical centroidal axis of each pier with the lines forming a 30° angle from the corners of the adjacent openings as illustrated in Fig. 5 (a) [61].

In different studies, it was assumed that spandrel elements remained elastic throughout the analysis due to the high dependency of this element on different parameters (i.e., the type of lintel, effective interlocking length etc.), and failure is assumed to occur in piers [19,42,60].

Nonlinear shear springs are assigned to the piers with an elastic axial stiffness (see Fig. 5 (b)). The spring element acts as a pure shear spring with a length equal to the height of a pier by tying the rotational degree of freedom and an elastic stiffness to represent the axial stiffness with the value of $\frac{EA}{h}$ for each pier. The initial in-plane stiffness of the nonlinear shear spring can be calculated based on Equation (3). Moreover, the maximum shear strength of each pier can be considered as the minimum value of the shear strength for the three failure modes for URM piers [21,50]. The maximum shear strength for the three failure modes can be obtained using the equations proposed in Table 2 [21,47,50].where f_{td} is the diagonal tensile strength of masonry, b is the width, t is the thickness of a pier, and ζ is the shear stress distribution coefficient at the center of a pier considering the aspect ratio calculated based on the equations in Table 3:

Moreover, the parameter α_0 is the zero-moment coefficient relevant to the moment distribution along with the height of a pier that should be defined by applying a static lateral load with a load pattern similar to the first mode of the building [21]. Then this parameter is calculated as the maximum value of the fraction of the height of a pier (H_0) with a positive or negative moment value as depicted in Fig. 5 (c) to the total height of a pier.

Table 1
Parameters and the corresponding equations for deriving the backbone curve of nonlinear shear spring of the UM and defining the hysteresis rules.

Parameter section	Parameter		Unperforated URM wall	Perforated URM wall
Backbone	α_y		$\frac{\sigma_0 + 0.0049f_c}{0.86\sigma_0 + 0.15f_c} \geq 0.4$	$\frac{0.81\sigma_0 + 0.043f_c}{\sigma_0 - 0.067f_c} \geq 0.4$
	η		0.14	0.19
	η_{soft}		$-0.168\frac{\sigma_0}{f_c} - 0.0168$	$-0.365\frac{\sigma_0}{f_c} - 0.01$
Hysteresis	pinching factor for strain during reloading		0.5	0.3
	pinching factor for stress during reloading	If $\frac{\sigma_0}{f_c} < 0.15$	0.8	0.3
		If $\frac{\sigma_0}{f_c} \geq 0.15$	0.6	0.25
	Damage due to energy		0.05	0.05
	Stiffness degradation factor due to ductility (β)		0.5	0.6

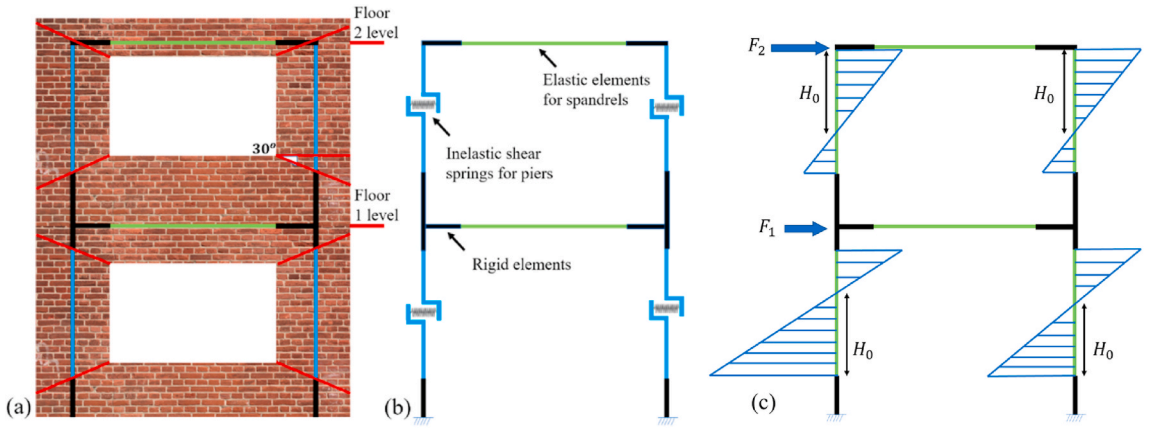

Fig. 5. (a) Discretization of a perforated URM wall to piers and spandrels based on Dolce's method, (b) schematic view of the wall modeled based on the CSM, and (c) moment distribution of the modeled wall subjected to lateral loadings as a sample.

Table 2
Equations for calculating the maximum shear strength of a URM wall based on shear sliding, diagonal cracking, and rocking failure modes.

Parameter (failure mode)	Equation
V_S (shear sliding)	$\left(\frac{f_{td}+0.4\sigma_0}{1+\frac{3\alpha_0 h f_{v0}}{\sigma_0 b}}\right)bt$
V_D (diagonal cracking)	$\frac{f_{td}bt}{\zeta}\sqrt{1+\frac{\sigma_0}{f_{td}}}$
V_R (rocking)	$\frac{\sigma_0}{2\alpha_0 h}\left(1-\frac{\sigma_0}{0.85f_c}\right)b^2t$

Table 3
Equations for deriving ζ (the shear stress distribution coefficient at the center of a pier considering the aspect ratio).

Aspect ratio	Shear stress distribution coefficient
$\frac{h}{b}\leq 1 \rightarrow$	$\zeta = 1$
$1<\frac{h}{b}<1.5 \rightarrow$	$\zeta = \frac{h}{b}$
$\frac{h}{b}\geq 1 \rightarrow$	$\zeta = 1.5$

2.2.1. Validation of the CSM

A full-scale two-story perforated URM wall as illustrated in Fig. 6 (a) was tested at the University of Pavia, and cyclic prescribed displacements as shown in Fig. 6 (b) were applied to the first and second floors with a ratio of 0.65 [62]. Fig. 6 (c) shows the stress-strain curve of the masonry material used in the experimental test with $f_{td} = 0.21$ MPa and $f_{v0} = 0.345$ MPa based on the material properties presented in Ref. [62]. The wall was modeled using CSM and the phenomenological laws of the unperforated URM walls presented in Table 1 (as utilized in the UM [48]) could be applied to each pier's nonlinear shear spring. However, the β factor was considered to be 0.6, and the accuracy of this assumption was investigated by comparing the test and numerical results.

A displacement control analysis using a Modified-newton solution algorithm was performed, and the convergence was controlled by means of an energy convergence test with a tolerance of 10^{-4}. The results were plotted as the base shear versus the roof displacement and compared with the test result in Fig. 6 (d) [62]. The comparison of the CSM results with the experimental data shows a good match in terms of roof displacement and base shear that confirms the use of the phenomenological laws of the unperforated URM walls utilized in the UM with manipulation of β factor.

3. Development and validation of the novel macroelement

Defining critical components is not possible in the UM, and a conservative procedure is considered for deriving the maximum shear strength of the perforated wall. In the CSM, detecting the critical components is possible, but the failure of a perforated wall is assumed to occur due to the piers assuming a linear element for the spandrels. Moreover, N-M interaction has not been considered in the CSM since all nonlinear behavior has been concentrated in a nonlinear shear spring. Considering similar hysteresis rules for both shear and flexural failure modes is another limitation of the CSM. To tackle all the limitations by keeping the simplicity of modeling, stability in

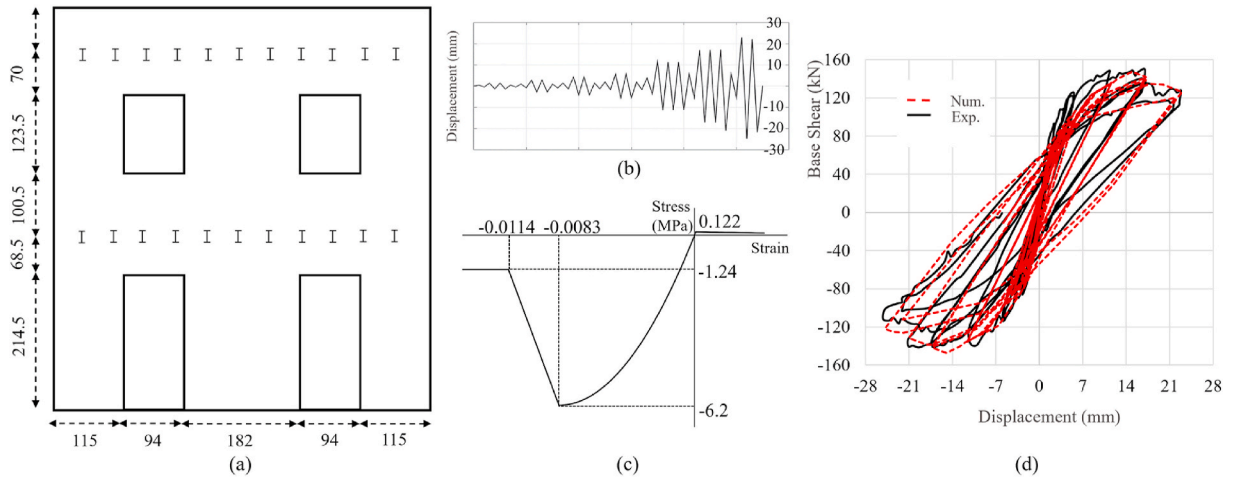

Fig. 6. (a) Geometry of the Pavia door wall, (b) cyclic displacement protocol of the test, (c) stress-strain curve of masonry [62], and (d) experimental-numerical comparison curves of the walls.

analysis, and efficiency in terms of the computational effort, a novel macroelement has been proposed and validated against the test results in this section.

3.1. Multiple vertical line element method (MVLEM)

The MVLEM element is available in the OpenSees framework [53] utilized to define the exact axial-flexural and shear behavior of a URM structural component with a high level of convergence during the nonlinear analyses and less computational effort [51,63]. The MVLEM element comprises multiple vertical nonlinear uniaxial fibers (nonlinear truss elements) that connect the upper and lower rigid elements, whereas the shear response is simulated by a shear spring located at height *ch* from the bottom of the wall element as depicted in Fig. 7 (a) [56]. The rotation of the wall due to axial-flexural loadings and transverse displacement due to the shear spring occurs independently and is summed up as the lateral displacement of a wall with fixed-free boundary conditions as highlighted in Fig. 7 (a) [56]. The MVLEM element has been utilized for the nonlinear analysis of flexural behavior dominated reinforced concrete walls and verified against the test walls with fixed-free boundary conditions [51,52,63]. Although, for employing the MVLEM elements in fixed-free boundary conditions, a sensitivity analysis should be done to investigate the most efficient number of elements that can predict the plastic hinge length. But, in order to implement an exact enough shear behavior formulation that is common for URM with the minimum number of elements for the fixed-fixed boundary conditions, modifications and new formulations are needed.

In order to simulate the pure axial-flexural behavior of a wall by neglecting shear behavior, the MVLEM undergoes modification. For this purpose, the rotational center of the MVLEM element is considered at the end of the element as illustrated in Fig. 7 (b). Furthermore, the first degree of freedom of the spring, the horizontal transition, must be rigid, with all other degrees (two and three) free.

3.2. Double modified multiple vertical line element method (DM-MVLEM)

In order to implement an explicit shear behavior formulation for URM walls, double modified MVLEMs (DM-MVLEM) are connected via a nonlinear shear spring, and two modified MVLEM elements are tied with a rigid connection in other degrees of freedom, as illustrated in Fig. 8 (a). Fig. 8 (b) shows fixed-fixed, and fixed-free boundary conditions and Fig. 8 (c) illustrates the kinematics of the novel macroelement subjected to lateral and compressive loadings in fixed-fixed and fixed-free boundary conditions. Therefore, the novel element can predict the actual flexural and shear behavior of URM components in both fixed-fixed and fixed-free boundary conditions by means of two MVLEM elements.

The stress-strain constitutive law of masonry is assigned to each uniaxial fiber, and for the shear constitutive law, shear sliding and

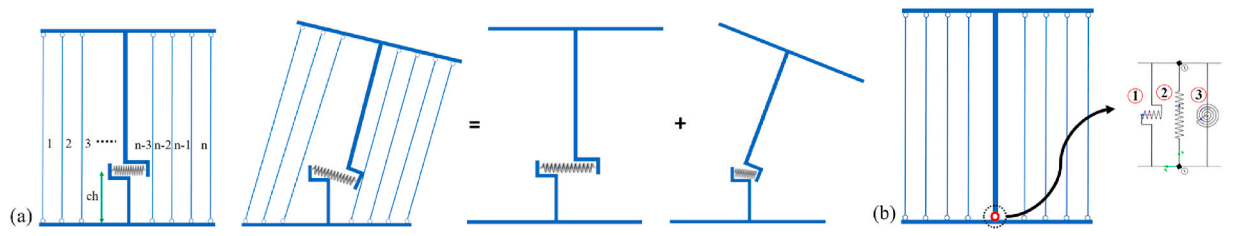

Fig. 7. (a) Kinematics of the conventional MVLEM element subjected to lateral and axial (compression) loadings, and (b). the modified MVLEM element for developing the macroelement to nonlinear modeling of URM buildings.

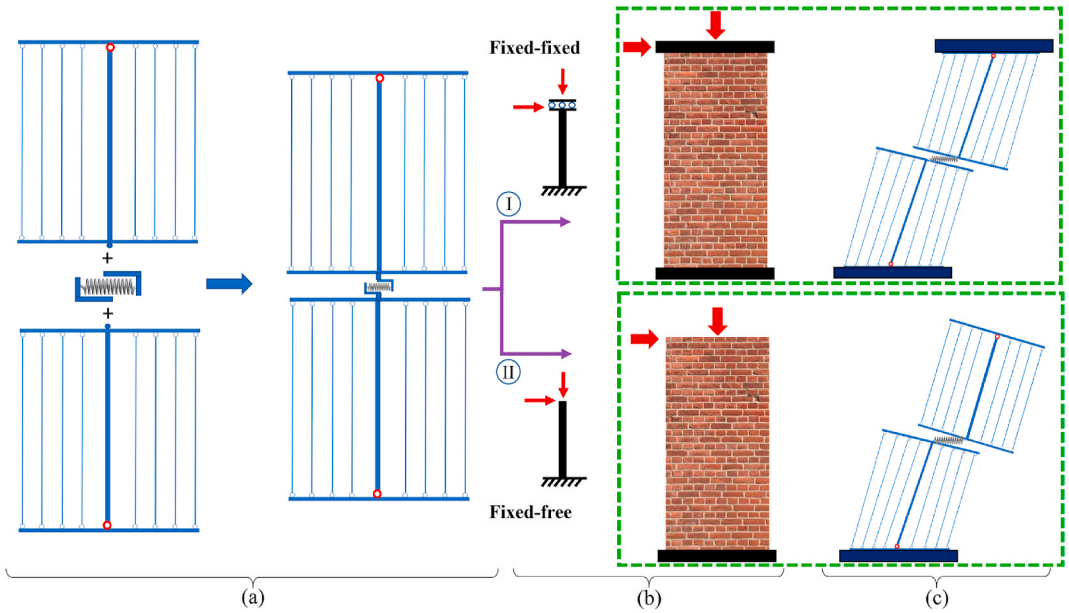

Fig. 8. (a) The DM-MVLEM macroelement composing two modified MVLEM element and a nonlinear shear spring at the middle, (b) fixed-fixed and fixed-free boundary conditions of URM walls, and (c) the kinematics of the novel macroelement with the two mentioned boundary conditions subjected to lateral and axial loadings.

diagonal cracking failure modes are considered since the fiber elements represent the flexural failure mode. For the mechanical properties of the nonlinear shear spring, the maximum shear strength can be determined as the minimum value of V_S and V_D based on the equations in Table 2, and the initial stiffness is derived based on Equation (5) since this spring only contributes to the shear behavior of the element [21,50].

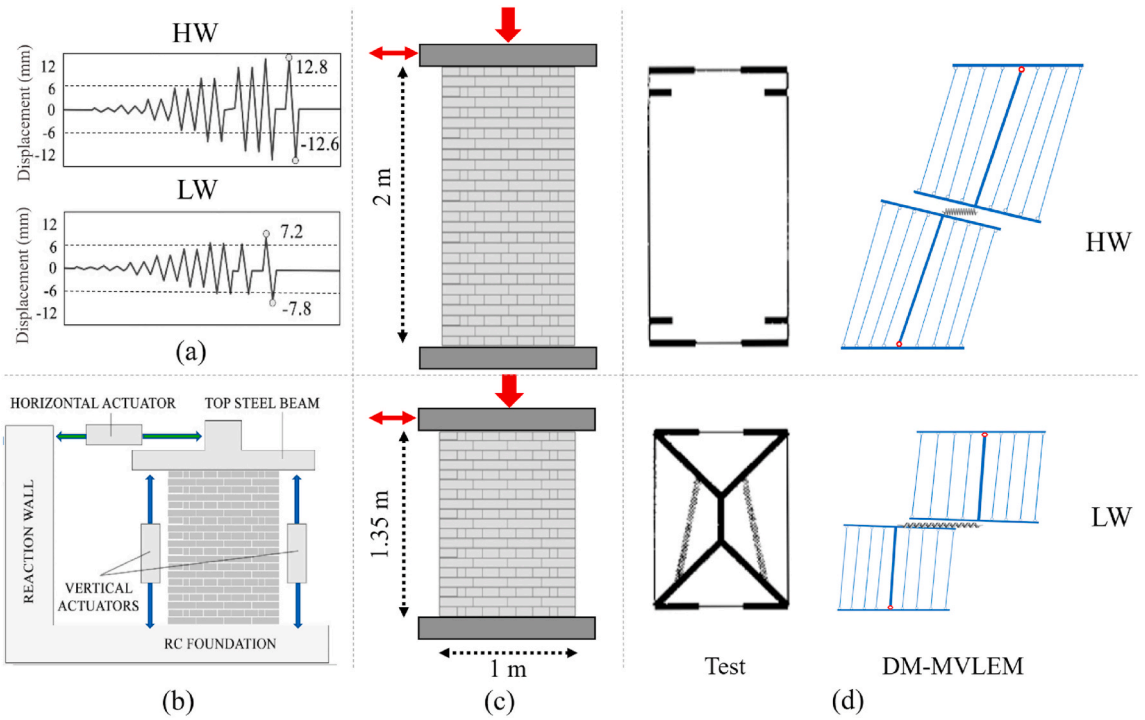

Fig. 9. (a) Displacement protocols applied to the HW and LW specimen, (b) experimental test setup [11], (c) geometry of the HW and LW, (d) the crack patterns (failure mode) based on the test results and kinematics of the DM-MVLEM models of the walls [32].

$$K_{Es} = \frac{GA}{1.2h} \tag{5}$$

The DM-MVLEM can be utilized for modeling spandrels by presenting new constitutive laws based on the experimental tests for the nonlinear shear spring. A macro-model was developed by employing the Euler-Bernoulli beam since Timoshenko's shear contribution is simulated in the shear spring at the middle of the macroelement [64]. For this purpose, the modified MVLEM elements are employed as an alternative to the Euler-Bernoulli beam (similar to modeling pier elements), and a nonlinear shear spring is implemented at the middle of the spandrel.

The maximum shear strength of the shear spring is derived as the minimum value of the V_D (diagonal cracking) derived from the equation in Table 2 and the interlocking strength at bed joints at the intersection between spandrel and piers (V_I) [65] which is:

$$V_I = \frac{f_{teq} th_{sp}^{\ 2}}{3L} \tag{6}$$

where h_{sp} is the spandrel's depth without lintel, and f_{teq} represents the equivalent tensile resistance due to interlocking, which is calculated based on:

$$f_{teq} = \frac{b_{eff}}{b_h}\left(f_{v0} + 0.65\sigma_p\right) \tag{7}$$

where b_{eff} is the effective interlocking length and b_h is the thickness of a brick plus a mortar joint, and σ_p corresponds to the vertical compressive stress in the adjacent piers [64,65].

3.2.1. Validation of piers modeled with the DM-MVLEM

To validate the DM-MVLEM, two URM walls with two different (shear and rocking) failure mechanisms were modeled based on the experimental tests presented in Refs. [32,66]. A constant vertical load of 150 kN was applied on top, and a quasi-static static test was done by applying a lateral cyclic displacement, as illustrated in Fig. 9 (a). Fig. 9 (b) shows the test setup for performing the quasi-static on the double clamped URM wall. The two-wythe clay-brick walls with the same thickness of 25 cm but different heights (see Fig. 9 (c)) were modeled with the DM-MVLEM. The material properties of the wall are similar to the Pavia door wall as presented in Ref. [32]. In the OpenSees framework, Concrete02 material has been utilized to model the fibers with the stress-strain curve based on the material properties presented in Ref. [32], and the Hysteretic material was utilized to model the trilinear shear spring as illustrated in Fig. 3 (d). Values utilized to derive the trilinear curve of the shear spring are presented in Table 4 based on [46,47,50], and the validity was investigated.

As illustrated in Fig. 9 (d), rocking failure mode with large horizontal cracks at the two ends of the wall occurs in the high wall (HW) test specimen [32]. The DM-MVLEM model of the HW indicates that the fiber elements are involved, and the deformation of the fibers is dominant compared to the deformation of the shear spring. Moreover, the test result shows the diagonal shear failure mode in the low wall (LW) specimen [32]. The contribution of the shear spring deformation of the DM-MVLEM model of the wall is more than the fiber elements that shows the shear failure mode. Therefore, the DM-MVLEM can predict both flexural and shear failure modes when compared with the test results.

The results of the displacement control analyses for the walls are depicted in Fig. 10 and compared with the experimental tests' results. Fig. 10 shows that the LW is characterized by wide cycles; the HW represents smaller cycles with lower dissipative capacity compared to the LW. The numerical-experimental comparison for both walls indicates that the DM-MVLEM provides an accurate enough estimation of shear capacity and cyclic behavior for the walls with specific failure mechanisms.

3.2.1.1. Comparative study of the accuracy of the DM-MVLEM. In order to compare the accuracy and efficiency of the novel DM-MVLEM element, results of the pushover analysis of the LW and HW specimens were carried out based on different modeling approaches and the results were compared with the test backbone curve result. Pushover analysis results of models developed using five, ten, and twenty MVLEM elements connected vertically with the nodes at the endings, as well as the CSM macroelement are depicted in Fig. 11 for both walls. Furthermore, FE analysis results were derived for the walls with Total strain crack material (TSCM) and Engineering masonry material (EMM) models in DIANA FEA software [51,67] plotted in Fig. 11. Compared with the TSCM, a shear failure mechanism based on the standard Coulomb friction failure criterion is included in the EMM model.

Initial stiffness, loading capacity, and post-peak stiffness are three main parameters for predicting the bilinear pushover curve of

Table 4
The values of the parameters utilized for defining the backbone curve of nonlinear shear spring for piers in the DM-MVLEM and the corresponding hysteresis rules.

parameters	Values
d_m	$0.0015h$
d_u	$0.01h$
V_u	$0.2V_m$
Pinching factor for strain during reloading	0.4
Pinching factor for stress during reloading	0.2
Damage due to energy	0.05
β	0.75

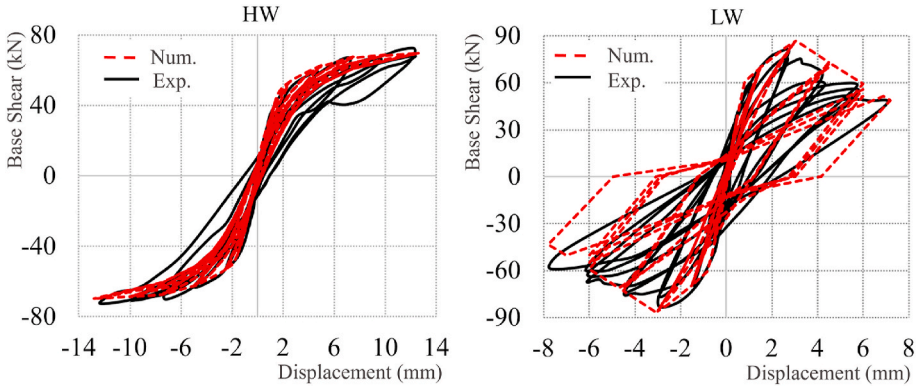

Fig. 10. Experimental-numerical comparison curves of the HW and LW walls.

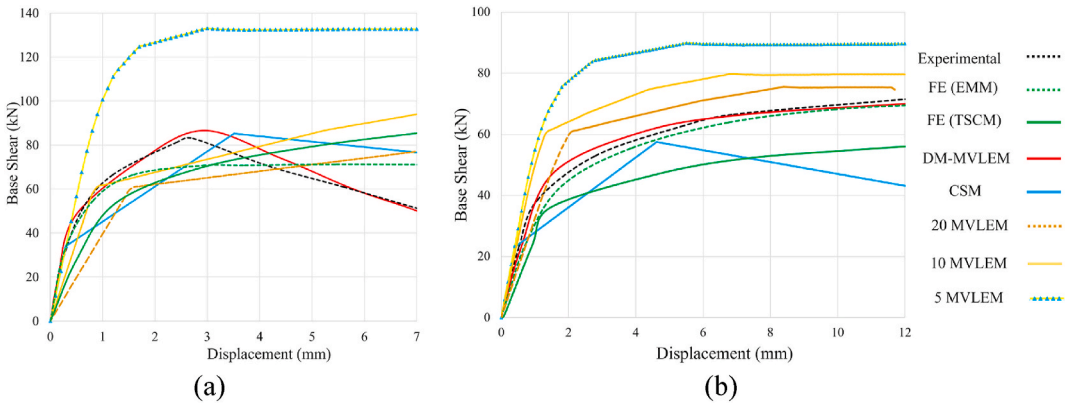

Fig. 11. POA results of the (a) LW and (b) HW modeled based on various modeling strategies and the backbone curve of the tests' results.

URM buildings. Backbone curves of the test result are considered as references and based on Fig. 11, the percent error values of the initial stiffness, loading capacity, and post-peak stiffness of various numerical simulations are presented in Fig. 12 (a) and (b) for the LW and HW specimens respectively. Note that the percent error value equals to the absolute error value divided by the test results' values. The average of percent error values that might not be a robust enough parameter for evaluating each numerical method are calculated and presented in Fig. 12 (c) for each wall to summarize the detailed results of Fig. 12 (a) and (b) and facilitate the comparative study. It can be pointed out that among the FE models, EMM is more accurate compared to the TSCM for the prediction of the load-bearing behavior and the damage pattern [67]. The CSM can predict the lateral load-bearing behavior of the LW with shear failure behavior with a good agreement but with a poor agreement for the HW with flexural failure mode. The poor agreement is shown for the backbone properties of the specimens modeled with the MVLEM elements; however, the loading capacity of the HW is in a good agreement with the test results and the error value is decreased by increasing the number of MVLEM elements [68]. The results of the models with MVLEM elements are sensitive to the number of the elements in fixed-fixed boundary conditions, and failure mode prediction cannot be investigated for the models developed using MVLEM elements. Therefore, using MVLEM elements for the nonlinear analysis of URM walls is not recommended. The DM-MVLEM models show a good agreement with the test results for both walls so that the average of percent error values are less than 13% for both specimens. Although more computational effort is needed to analyze the FE models compared to the EFM approaches as reported in Refs. [2,29,69], a better correlation between the DM-MVLEM models and test results is concluded compared to the FE model with EMM.

3.2.2. Validation of a spandrel modeled with the DM-MVLEM

Validation of a spandrel using the DM-MVLEM was carried out based on a quasi-static cyclic test presented in Ref. [70]. A three-wythe clay-brick URM spandrel with a thickness of 38 cm was tested as shown in Fig. 13 (a) so that the pier (a) was fixed, but the pier (b) could move vertically. Moreover, the rotation of the two ends of the pier (a) was fixed during the analysis, and a constant uniform compressive stress of 0.5 MPa was applied on the piers [70]. Note that in the OpenSees framework, modeling the MVLEM macroelements in a horizontal direction is not possible; therefore, to simulate the spandrel elements, the modified MVLEM elements had to be modeled manually by employing nonlinear truss elements for modeling the fibers, rigid beam elements for the top and bottom of the element, and the twoNodeLink element available in OpenSees to connect the rigid top and bottom parts [53]. Moreover, two modified MVLEMs were connected using a zero-length element to represent the nonlinear shear behavior of the DM-MVLEM

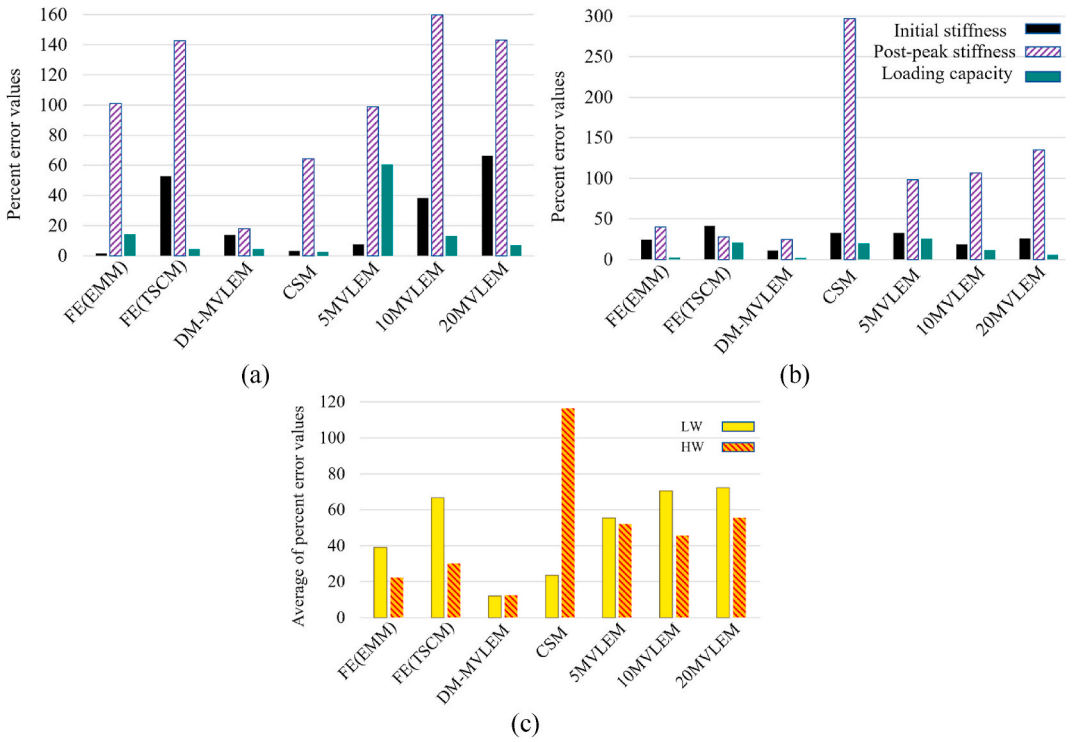

Fig. 12. Percent error values for the initial stiffness, post-peak stiffness, and loading capacity values for the (a) LW, (b) HW specimens, and (c) the average of the percent error values.

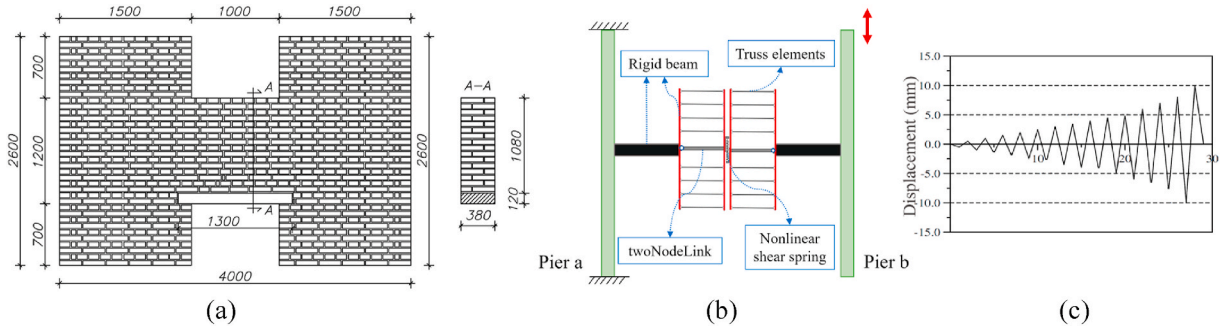

Fig. 13. (a) Geometry of the H shape model, (b) numerical model of the test specimen based on DM-MVLEM, and (c) displacement protocol applied to the specimen [70].

element. The numerical model developed using the DM-MVLEM and the displacement protocol applied vertically to the pier (b) has been illustrated in Fig. 13 (b) and (c).

The stress-strain constitutive law for masonry is depicted in Fig. 14 (a), and the values for f_{td} and f_{v0} are considered 0.19 MPa and 0.28 MPa, respectively based on [70]. Values for the pinching factors and damage due to energy are taken from Table 4, similar to the values for the masonry piers. Other parameters are summarized in Table 5 for defining the spandrels' nonlinear shear springs validated after the calibration process by plotting the experimental and numerical curves as depicted in Fig. 14 (b). Differences between the maximum shear strength and the initial stiffness of the test specimen and the numerical model are 1.3% and 9.7%, respectively.

3.2.3. Validation of a full-scale perforated wall modeled with the DM-MVLEM

In order to investigate the accuracy of the proposed method, the Pavia door wall (see Fig. 6) was modeled using the DM-MVLEM as illustrated in Fig. 15 (a), and the cyclic prescribed displacements were applied based on the experimental test [62]. Differences between the maximum shear strength and the initial stiffness of the test specimen and the numerical model are 5.2% and 11.7%, respectively. The comparison of test results and the numerical simulation, as illustrated in Fig. 15 (b), shows a good agreement between roof displacement and base shear.

Fig. 16 (a) shows the crack patterns and failure mechanisms of the Pavia door wall after performing the test. Combined diagonal

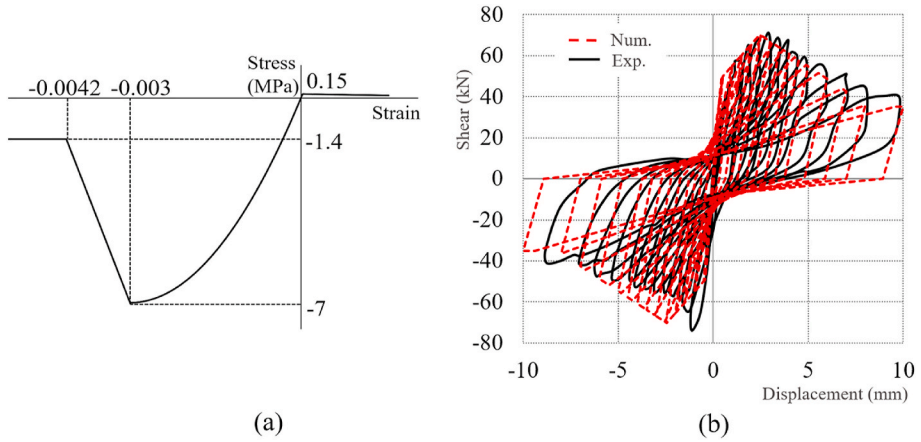

Fig. 14. (a) stress-strain curve of masonry based on the Concrete02 material, and (b) experimental-numerical comparison curves of the spandrel element.

Table 5
The values of the parameters utilized for defining the backbone curve of nonlinear shear spring for spandrels in the DM-MVLEM and the corresponding hysteresis rules.

Parameters	values
d_m	$0.002h$
d_u	$0.008h$
V_u	$0.5V_m$
B	0.5

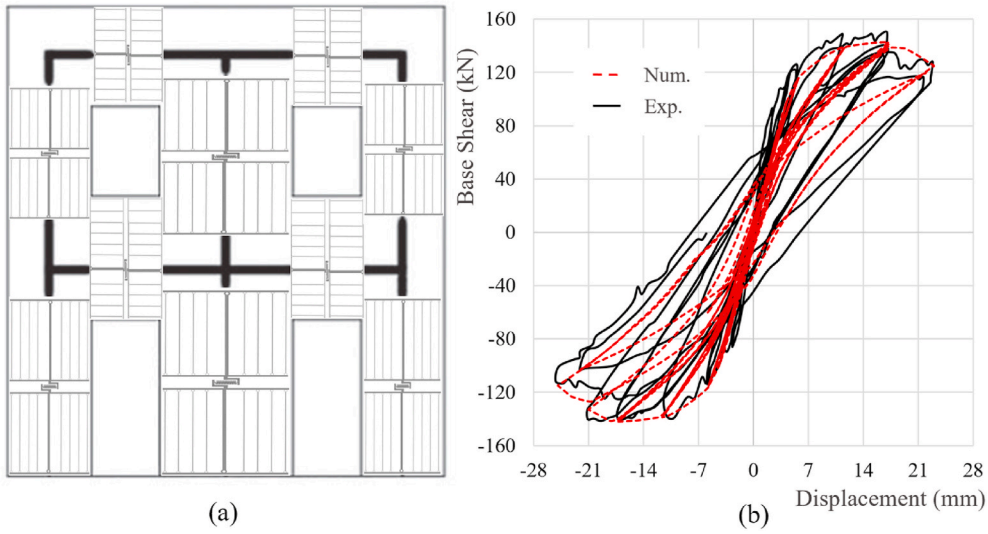

Fig. 15. (a) The developed model of the wall based on the DM-MVLEM and (b) experimental-numerical comparison curves of the perforated URM wall.

shear and flexural failure mechanisms cause the soft story in the first floor, with cracks visible in the spandrels of the first story. As illustrated in Fig. 16 (b), the DM-MVLEM is able to predict the failure mechanisms of the URM structural components in agreement with the results from the test. Failure of the fiber elements of the DM-MVLEM elements in the first story and the shear springs shows the mixed shear-flexural failure. Moreover, cracks in spandrel elements are predicted in the numerical model, as seen in the test.

In order to investigate the accuracy of the model developed using the DM-MVLEM when subjected to more realistic seismic events, incremental dynamic analysis (IDA) [71,72] of a single record was performed. The IDA results were compared to the pushover analyses results. Mass proportional and mode proportional load patterns were chosen for performing the POA to investigate their accuracy compared to the IDA results.

The results associated with Rayleigh damping based on mass and tangent (current) stiffness matrix and last committed stiffness show an approximate consistency based on [73]. Therefore, considering convergence issues and prolongation of analysis caused by

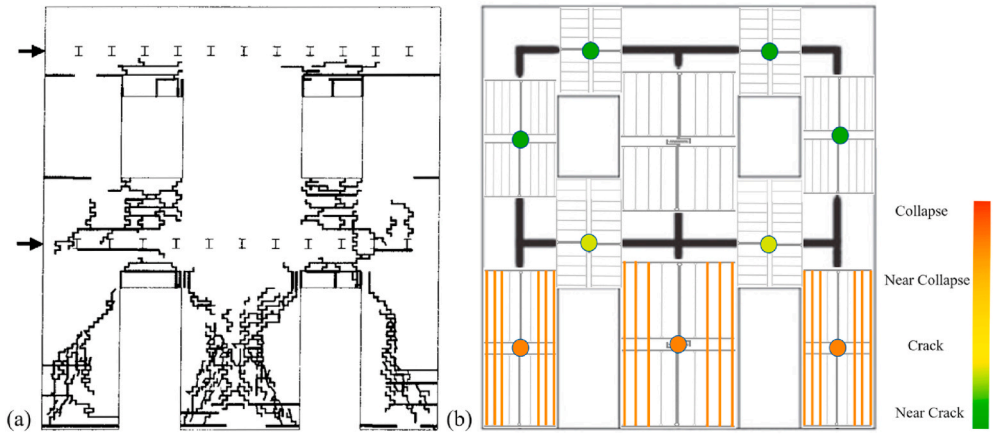

Fig. 16. (a) Crack patterns of the Pavia door wall at the end of the test, and (b) damage representation of the wall modeled with the DM-MVLEM.

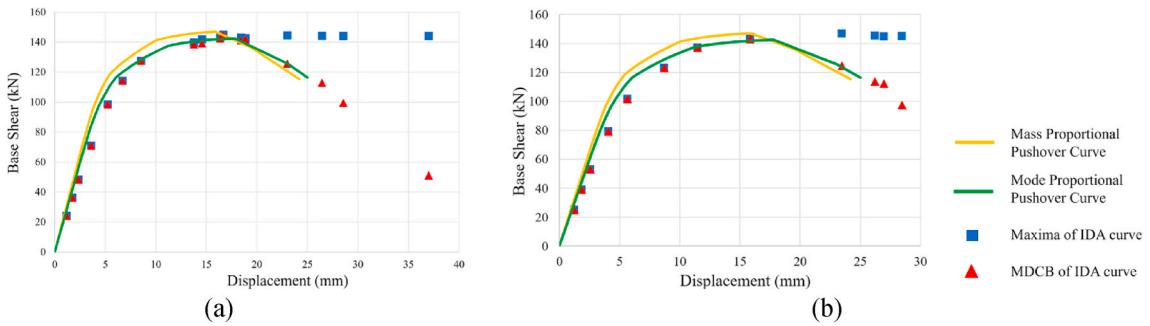

Fig. 17. Pushover curves of Pavia door wall based on mass-proportional and mode-proportional loading patterns and results from the IDA based on the Maxima and MDCB scenarios for the (a) Kobe and (b) Landers seismic records.

using the current stiffness matrix, it may be judicious to apply the committed stiffness matrix in lieu of the current stiffness matrix which results in saving computational time. An equivalent damping ratio of 2% at the first and second modal frequencies is considered [47] proportional to the mass and the last committed stiffness matrix for performing the IDA.

For performing the IDA, a seismic record was applied to the model, and the intensity of the record was increased. Two seismic records were chosen from the FEMA P-695 seismic records [74]. Fig. 17 (a) shows the diagram of base shear versus roof displacement resulting from the NTHA of the modeling subjected to the Kobe seismic record, which occurred in Japan with a magnitude of 6.9, and Fig. 17 (b) shows the results of the Landers record in the United States which had a magnitude of 7.3.

To investigate the most accurate process for the comparison, two scenarios were considered to illustrate the IDA results in the versatile OpenSees framework. For each record's result, maximum displacement and the corresponding base shear (MDCB) and the maxima of base shear and displacement curve (Maxima) were extracted, with the curves provided for the records, as illustrated in Fig. 17. The results of the Maxima and MDCB scenarios are not distinguishable before the peak base shear as shown in Fig. 17, but the

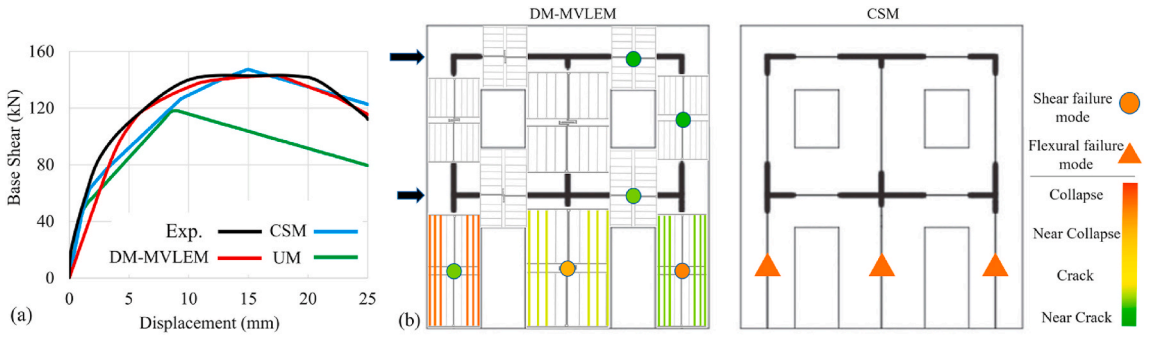

Fig. 18. (a) Pushover curve of the Pavia door wall developed based on the UM, CSM, and the DM-MVLEM and (b) damage representation of the Pavia door wall modeled using the DM-MVELM and CSM.

envelope curve of the results from the NTHA based on the Maxima scenario cannot reflect the post-peak degradation that the MDCB results can exhibit.

The mode proportional pushover curves are closer to the IDA envelope curves before the peak base shear due to the stiffness degradation and the damage due to energy. However, the mass proportional pushover curves can exhibit maximum base shear and the corresponding roof displacement in better agreement with the IDA results. As illustrated in Fig. 17, the post-peak degradation visible in both mode and mass proportional pushover curves is in good agreement with the results from the IDA based on the MDCB scenario, which shows the accuracy of this scenario for the evaluation of the accuracy of the pushover load patterns compared to the conventional Maxima scenario utilized in Refs. [18,21,50,60].

4. Seismic behavior of the full-scale wall modeled with the UM, CSM, and DM-MVLEM

The Pavia door wall as shown in Fig. 6 (a) was modeled using the UM, CSM, and DM-MVLEM as case study 1 for performing a comparative study. A comparative study is carried out to evaluate the performance of each method. Discussions of the results of the seismic analyses in this section are elaborated in the next section by emphasizing the characteristic of each modeling approach.

4.1. Pushover analysis

The POA was performed considering the load pattern of the test for the Pavia door wall to enable comparison of the results with the test results. The POA results of the CSM, and DM-MVLEM models are illustrated in Fig. 18 (a). As illustrated in Fig. 16, failure modes can be predicted in good agreement with the test results for the DM-MVLEM model during the cyclic displacement control analysis. In order to compare the failure modes occurring in the case study, the damage patterns for the model developed using the DM-MVLEM and CSM by performing a monotonic POA are illustrated in Fig. 18 (b) at the final prescribed displacement of the pushover curves.

4.2. Multiple records IDA

Twenty-two pairs of far-field seismic records from the FEMA-P 695 guideline [74] were chosen, and the IDA was done by increasing the intensity of the records until a limit state was reached. The inter-story drift of 1% was considered for the collapse limit state based on [38]. An IDA curve is a diagram of the ground motion intensity measure (IM) against an engineering demand parameter (EDP). The IM and EDP are the spectral acceleration corresponding to the first mode elastic vibration period of the structure considering 5% of damping ($Sa(T_1, 5\%)$), and the maximum inter-story drift respectively in this study [75]. Fig. 19 shows the result of the IDA of the case study modeled using the three methods.

To facilitate the comparison of the IDA results, the mean value of the IMs that cause an inter-story drift limit state to occur was derived and is summarized in Fig. 20. The first limit state is considered as the immediate occupancy (IO) with an inter-story drift of 0.3%, the second is life safety (LS) with an inter-story drift of 0.6%, and the third is collapse prevention with an inter-story drift of 1% based on [38].

5. Discussion

The main advantages of UM are that it obviates the need for the discretization of structural components (piers and spandrels), uses simple formulations for deriving the nonlinear spring parameters, requires less computational effort and results in a good convergence during the nonlinear analyses are the main advantages of the UM. However, using the EHM for deriving the initial in-plane stiffness of URM walls is approximate that cannot reflect the effects of the unsymmetrical openings. Furthermore, the equation for deriving the maximum shear strength considers the rocking and shear sliding failure modes for a perforated wall with a simplified conservative assumption and does not consider the failure mode of each pier separately. Since a perforated wall is not discretized into piers and spandrels, the most critical structural components cannot be detected using the UM approach.

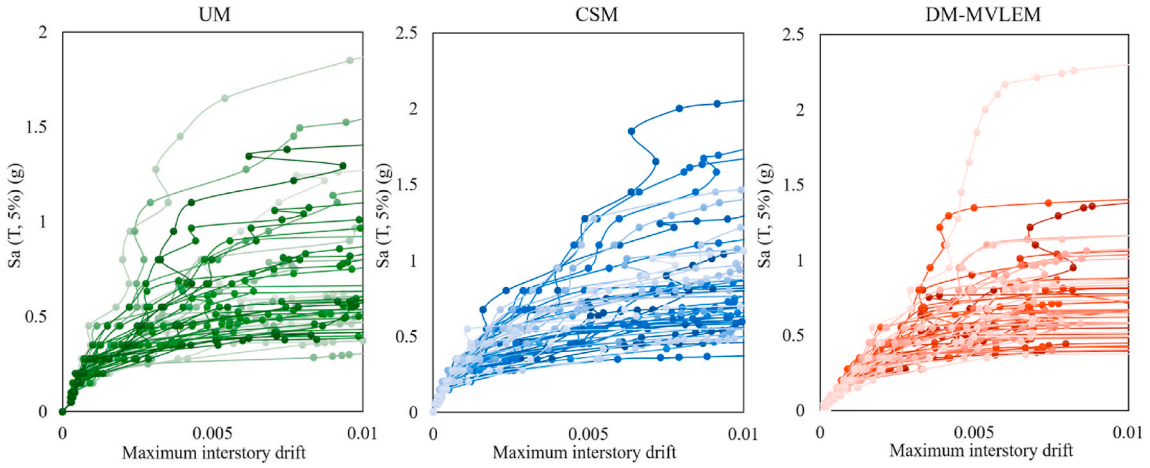

Fig. 19. IDA curves of the Pavia door wall modeled based on the UM, CSM and DM-MVLEM.

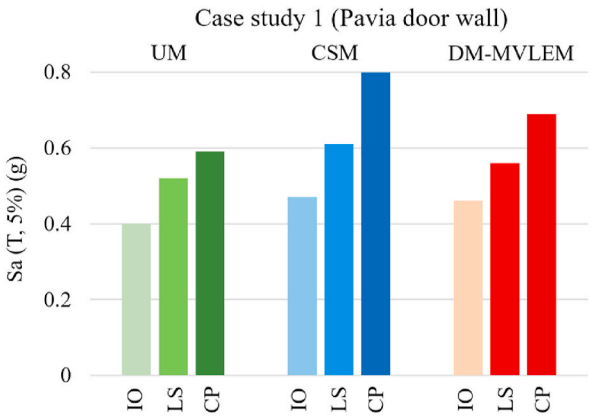

Fig. 20. The mean values of IMs that cause the IO, LS and CP limit states to occur in the case study modeled based on the UM, CSM and DM-MVLEM.

By discretizing the piers and spandrels through the modeling and calculating the maximum shear strength based on three failure modes of piers, the most probable failure mode of each pier, as well as cracked or damaged components that cannot be predicted using the UM can be detected using the CSM. However, concentrating all the failure behavior of the wall (flexural and shear modes) in a single shear spring is not realistic enough. Considering the same deformation limits and the same hysteresis rule for the piers with rocking and shear failure modes is another limitation of this method. Moreover, N-M interaction and the effect of a fluctuating axial force on the strength and stiffness of the components are not investigated in the CSM. Furthermore, a reliable method for modeling spandrels is needed to investigate the effect of this structural component on the results. The DM-MVLEM is an alternative to tackle the limitations and maintain simplicity, efficiency in computations, and stability during the nonlinear analyses. The main features of the methods and FE method using EMM [67,76] are synthesized in Table 6 to facilitate comparison.

A comparative study was carried out on the nonlinear analyses' results of the Pavia door wall developed using the UM, CSM and DM-MVLEM. The POA results show good agreement of the CSM and DM-MVLEM with the test results for deriving the pushover curve (see Fig. 18 (a)). However, due to the conservative approach of the UM for calculating the maximum shear strength by assuming weak connections of spandrels to piers, the pushover curve is derived conservatively compared to the test. The damage patterns for the Pavia door wall show that the CSM model cannot reflect the combined shear-flexural failure mode, as seen in the test. Therefore, the diagonal shear failure mode that can be seen in the test cannot be seen in the CSM model. Nevertheless, the damage pattern is predicted with a good agreement to the test results using the DM-MVLEM model, as illustrated in Fig. 18 (b). The results of the IDA show that the DM-MVLEM reflects a more conservative approach in terms of hysteresis rules compared to the CSM since the pushover curves are close to each other, but the mean acceleration values for the IO and CP limit states as shown in Fig. 20 are less than in the CSM. Moreover, as expected from the pushover curves the UM yields the most conservative results in the IDA.

6. Conclusion

Various simplified methods have been developed for the nonlinear modeling of URM buildings to perform seismic analysis with sufficient speed and accuracy. The UM is a simplified method that is considered the most efficient method reviewed and modified by

Table 6
Comparison of the main features of the UM, CSM, and DM-MVLEM.

Feature section	Feature	UM	CSM	DM-MVLEM	FEM (EMM)
Modeling and calculation	Discretization of the structural components	×	✓	✓	×
	Consideration of N-M interaction	×	×	✓	✓
	Consideration of N-V interaction	×	×	×	✓
	Stress-strain curve input data	×	×	✓	✓
	Explicit hysteresis behavior for different in-plane failure modes	×	×	✓	✓
	Combined in-plane and out-of-plane response	×	×	×	✓
In-plane failure mechanisms	Soft story	✓	✓	✓	✓
	Flexural failure mode of piers	×	✓	✓	✓
	Shear failure mode of piers	×	✓	✓	✓
	Flexural failure mode of spandrels	×	×	✓	✓
	Shear failure mode of spandrels	×	×	✓	✓
	Combined flexural and shear failure modes	×	×	✓	✓
Type of analyses	Modal analysis	✓	✓	✓	✓
	Static linear	✓	✓	✓	✓
	Nonlinear pushover	✓	✓	✓	✓
	Nonlinear dynamic	✓	✓	✓	✓
	Local collapse analysis	×	×	×	×
Availability	Availability in openaccess or opensource software	✓	✓	✓	×

employing accurate enough EHM to derive the initial in-plane stiffness of perforated URM walls. But in a more detailed approach, the CSM is entailing a model of a perforated wall with nonlinear shear springs for the piers, with the linear spandrels. Definite equations for deriving the maximum shear strength of the piers were utilized for different failure modes, and the accuracy of using phenomenological laws of the unperforated URM walls presented in the UM with manipulation was investigated through the validation process.

To tackle the limitations of the UM and CSM and maintain simplicity in modeling, efficiency in computational efforts, and stability during nonlinear analyses, a novel macroelement is developed using the MVLEM element available in the OpenSees framework. The new macroelement consists of two modified MVLEMs to reflect the axial-flexural behavior of the wall connected via a nonlinear shear spring at the middle. The DM-MVLEM is validated against the experimental tests results on piers, a spandrel, and a full-scale perforated URM wall. Results of the POA of two piers with different modeling strategies show that MVLEM cannot reflect the actual behavior of URM piers, but the DM-MVLEM can predict the real behavior of the piers with good agreements with the tests' results. Even more correlation between the DM-MVELM and tests' results is concluded compared to the FE model using EMM with more computational effort. In order to investigate the accuracy of the DM-MVLEM subjected to dynamic loading and detect the most accurate load pattern for performing the POA, the results of the IDA for the Maxima and MDCB scenarios of two seismic records have been plotted against the mode proportional and mass proportional POA results. The results show that the IDA results of the Maxima and MDCB are indistinguishable before and including the point with the maximum base shear strength, but after that point, the envelope curve of the MDCB can reflect the post-peak degradation that cannot be seen for the Maxima curve. Hence, compared to the conventional Maxima scenario, the MDCB scenario can be a more realistic way to plot the IDA curves and compare the POA and IDA results.

A study was conducted to compare the seismic behavior of the Pavia door wall case study developed using the three aforementioned modeling approaches. The results from the POA show a good agreement of the CSM and DM-MVLEM with the experimental test results. The damage pattern is predicted by the DM-MVLEM in good agreement with the test. Nevertheless, the combined flexural and shear failure modes detected in the test are not predicted by the CSM. The IM values derived from the IDA of CSM and DM-MVLEM are close to each other for IO and LS limit states, but the DM-MVLEM is on the safe side in predicting the occurrence of the CP limit state.

The UM can be utilized as a fast tool for seismic analysis of ordinary URM buildings with conservative results. Given that not only the global analysis results but also detection of the most critical component are crucial, the CSM can be an accurate enough alternative for modeling the URM buildings without weak spandrels compared to the pier elements. The novel DM-MVLEM is an accurate enough method to predict the combined shear and flexural failure modes, nonlinear behavior of spandrel elements, and capture the N-M interaction effects. Future studies are required to improve the load-bearing behavior of the DM-MVLEM by implementing a new formulation to consider the N-V interaction during the analysis. Moreover, the element can be utilized for the nonlinear modeling of reinforced masonry walls.

Credit author statement

Amirhosein Shabani Conceptualization; Methodology; Investigation; Resources; Data Curation; Writing - Original Draft; Visualization;

Mahdi Kioumarsi Conceptualization; Writing - Review & Editing; Supervision; Project administration; Funding acquisition.

Declaration of competing interest

The authors declare that they have no known competing financial interests or personal relationships that could have appeared to influence the work reported in this paper.

Acknowledgements

This work is a part of the HYPERION project. HYPERION has received funding from the European Union's Framework Programme for Research and Innovation (Horizon 2020) under grant agreement No 821054. The contents of this publication are the sole responsibility of Oslo Metropolitan University (Work Package 5, Task 2) and do not necessarily reflect the opinion of the European Union.

References

[1] A.M. D'Altri, V. Sarhosis, G. Milani, J. Rots, S. Cattari, S. Lagomarsino, et al., Modeling strategies for the computational analysis of unreinforced masonry structures: review and classification, Arch. Comput. Methods Eng. (2019) 1–33, https://doi.org/10.1007/s11831-019-09351-x.

[2] A. Shabani, M. Kioumarsi, M. Zucconi, State of the art of simplified analytical methods for seismic vulnerability assessment of unreinforced masonry buildings, Eng. Struct. 239 (2021), 112280, https://doi.org/10.1016/j.engstruct.2021.112280.

[3] A. Aşıkoğlu, G. Vasconcelos, P.B. Lourenço, B. Pantò, Pushover analysis of unreinforced irregular masonry buildings: lessons from different modeling approaches, Eng. Struct. 218 (2020), 110830, https://doi.org/10.1016/j.engstruct.2020.110830.

[4] P. Roca, M. Cervera, G. Gariup, Structural analysis of masonry historical constructions. Classical and advanced approaches, Arch. Comput. Methods Eng. 17 (2010) 299–325, https://doi.org/10.1007/s11831-010-9046-1.

[5] F. Romano, M.S. Alam, M. Zucconi, M. Faggella, A.R. Barbosa, B. Ferracuti, Seismic demand model class uncertainty in seismic loss analysis for a code-designed URM infilled RC frame building, Bull. Earthq. Eng. 19 (2021) 429–462, https://doi.org/10.1007/s10518-020-00994-x.

[6] M. Aschheim, E. Hernández-Montes, D. Vamvatsikos, Design of Reinforced Concrete Buildings for Seismic Performance: Practical Deterministic and Probabilistic Approaches, Taylor and Francis Group, 2019.

[7] M. Yekrangnia, P.G. Asteris, Multi-strut macro-model for masonry infilled frames with openings, J. Build. Eng. 32 (2020), 101683, https://doi.org/10.1016/j.jobe.2020.101683.

[8] A. Shabani, M. Kioumarsi, V. Plevris, H. Stamatopoulos, Structural vulnerability assessment of heritage timber buildings: a methodological proposal, Forests 11 (2020) 881, https://doi.org/10.3390/f11080881.

[9] E. Hernández-Montes, M.A. Fernández-Ruiz, M. Aschheim, L.M. Gil-Martín, Structural knowledge within the 6th century AD Arch of Taq-iKisra, Int. J. Architect. Herit. 11 (2017) 891–900, https://doi.org/10.1080/15583058.2017.1321699.
[10] E. Quagliarini, G. Maracchini, F. Clementi, Uses and limits of the Equivalent Frame Model on existing unreinforced masonry buildings for assessing their seismic risk: a review, J. Build. Eng. 10 (2017) 166–182, https://doi.org/10.1016/j.jobe.2017.03.004.
[11] D. Malomo, M.J. DeJong, A Macro-Distinct Element Model (M-DEM) for simulating the in-plane cyclic behavior of URM structures, Eng. Struct. 227 (2021), 111428, https://doi.org/10.1016/j.engstruct.2020.111428.
[12] P. Fajfar, A nonlinear analysis method for performance-based seismic design, Earthq. Spectra 16 (2000) 573–592, https://doi.org/10.1193/1.1586128.
[13] D. D'Ayala, A. Meslem, D. Vamvatsikos, K. Porter, T. Rossetto, Guidelines for analytical vulnerability assessment: low/mid-rise, GEM vulnerability and loss modelling, in: Global Earthquake Model, GEM) Foundation, Pavia, 2015.
[14] T.M. Ferreira, N. Mendes, R. Silva, Multiscale seismic vulnerability assessment and retrofit of existing masonry buildings, Buildings 9 (2019) 91, https://doi.org/10.3390/buildings9040091.
[15] A. Maria D'Altri, N. Lo Presti, N. Grillanda, G. Castellazzi, S. de Miranda, G. Milani, A two-step automated procedure based on adaptive limit and pushover analyses for the seismic assessment of masonry structures, Comput. Struct. 252 (2021), 106561, https://doi.org/10.1016/j.compstruc.2021.106561.
[16] H. Krawinkler, G.D.P.K. Seneviratna, Pros and cons of a pushover analysis of seismic performance evaluation, Eng. Struct. 20 (1998) 452–464, https://doi.org/10.1016/S0141-0296(97)00092-8.
[17] A. Shabani, A. Alinejad, M. Teymouri, A. Nascimento Costa, M. Shabani, M. Kioumarsi, Seismic vulnerability assessment and strengthening of heritage timber buildings: a review, Buildings 11 (2021) 661, https://doi.org/10.3390/buildings11120661.
[18] Y. Endo, L. Pelà, P. Roca, Review of different pushover analysis methods applied to masonry buildings and comparison with nonlinear dynamic analysis, J. Earthq. Eng. 21 (2016) 1234–1255, https://doi.org/10.1080/13632469.2016.1210055.
[19] L. Pasticier, C. Amadio, M. Fragiacomo, Non-linear seismic analysis and vulnerability evaluation of a masonry building by means of the SAP2000 V. 10 code, Earthq. Eng. Struct. Dynam. 37 (2008) 467–485, https://doi.org/10.1002/eqe.770.
[20] C. Chácara, F. Cannizzaro, B. Pantò, I. Caliò, P.B. Lourenço, Assessment of the dynamic response of unreinforced masonry structures using a macroelement modeling approach, Earthq. Eng. Struct. Dynam. 47 (2018) 2426–2446, https://doi.org/10.1002/eqe.3091.
[21] S. Petrovčič, V. Kilar, Seismic failure mode interaction for the equivalent frame modeling of unreinforced masonry structures, Eng. Struct. 54 (2013) 9–22, https://doi.org/10.1016/j.engstruct.2013.03.050.
[22] D. Baraldi, A. Cecchi, A full 3D rigid block model for the collapse behaviour of masonry walls, Eur. J. Mech. Solid. 64 (2017) 11–28, https://doi.org/10.1016/j.euromechsol.2017.01.012.
[23] G. Milani, S. Casolo, A. Naliato, A. Tralli, Seismic assessment of a medieval masonry tower in Northern Italy by limit, nonlinear static, and full dynamic analyses, Int. J. Architect. Herit. 6 (2012) 489–524, https://doi.org/10.1080/15583058.2011.588987.
[24] G. Milani, Fast vulnerability evaluation of masonry towers by means of an interactive and adaptive 3D kinematic limit analysis with pre-assigned failure mechanisms, Int. J. Architect. Herit. 13 (2019) 941–962, https://doi.org/10.1080/15583058.2019.1645241.
[25] F.P.A. Portioli, Rigid block modelling of historic masonry structures using mathematical programming: a unified formulation for non-linear time history, static pushover and limit equilibrium analysis, Bull. Earthq. Eng. 18 (2020) 211–239, https://doi.org/10.1007/s10518-019-00722-0.
[26] F. Cannizzaro, B. Pantò, S. Caddemi, I. Caliò, A Discrete Macro-Element Method (DMEM) for the nonlinear structural assessment of masonry arches, Eng. Struct. 168 (2018) 243–256, https://doi.org/10.1016/j.engstruct.2018.04.006.
[27] M. Malena, F. Portioli, R. Gagliardo, G. Tomaselli, L. Cascini, G. de Felice, Collapse mechanism analysis of historic masonry structures subjected to lateral loads: a comparison between continuous and discrete models, Comput. Struct. 220 (2019) 14–31, https://doi.org/10.1016/j.compstruc.2019.04.005.
[28] A. Fortunato, F. Fabbrocino, M. Angelillo, F. Fraternali, Limit analysis of masonry structures with free discontinuities, Meccanica 53 (2018) 1793–1802, https://doi.org/10.1007/s11012-017-0663-8.
[29] N. Grillanda, M. Valente, G. Milani, A. Chiozzi, A. Tralli, Advanced numerical strategies for seismic assessment of historical masonry aggregates, Eng. Struct. 212 (2020), 110441, https://doi.org/10.1016/j.engstruct.2020.110441.
[30] F. Portioli, C. Casapulla, L. Cascini, An efficient solution procedure for crushing failure in 3D limit analysis of masonry block structures with non-associative frictional joints, Int. J. Solid Struct. 69–70 (2015) 252–266, https://doi.org/10.1016/j.ijsolstr.2015.05.025.
[31] H. Pirsaheb, M.J. Moradi, G. Milani, A Multi-Pier MP procedure for the non-linear analysis of in-plane loaded masonry walls, Eng. Struct. 212 (2020), 110534, https://doi.org/10.1016/j.engstruct.2020.110534.
[32] G. Magenes, G.M. Calvi, In-plane seismic response of brick masonry walls, Earthq. Eng. Struct. Dynam. 26 (1997) 1091–1112, https://doi.org/10.1002/(sici)1096-9845(199711)26:11<1091::aid-eqe693>3.0.co;2-6.
[33] M. Yekrangnia, A. Bakhshi, M.A. Ghannad, Force-displacement model for solid confined masonry walls with shear-dominated failure mode, Earthq. Eng. Struct. Dynam. 46 (2017) 2209–2234, https://doi.org/10.1002/eqe.2902.
[34] J.V. Lemos, Discrete element modeling of masonry structures, Int. J. Architect. Herit. 1 (2007) 190–213, https://doi.org/10.1080/15583050601176868.
[35] B. Pulatsu, E. Erdogmus, P.B. Lourenço, J.V. Lemos, K. Tuncay, Simulation of the in-plane structural behavior of unreinforced masonry walls and buildings using DEM, Structures 27 (2020) 2274–2287, https://doi.org/10.1016/j.istruc.2020.08.026.
[36] M. Mistler, A. Anthoine, C. Butenweg, In-plane and out-of-plane homogenisation of masonry, Comput. Struct. 85 (2007) 1321–1330, https://doi.org/10.1016/j.compstruc.2006.08.087.
[37] F. Greco, P.B. Lourenço, Seismic assessment of large historic vernacular adobe buildings in the Andean Region of Peru. Learning from Casa Arones in cusco, J. Build. Eng. 40 (2021), 102341, https://doi.org/10.1016/j.jobe.2021.102341.
[38] FEMA, Prestandard and Commentry for the Seismic Rehabilitaion of Buildings, FEMA 356, Federal Emergency Management Agency, Washington, D.C., 2000.
[39] S. Lagomarsino, A. Penna, A. Galasco, S. Cattari, TREMURI program: an equivalent frame model for the nonlinear seismic analysis of masonry buildings, Eng. Struct. 56 (2013) 1787–1799, https://doi.org/10.1016/j.engstruct.2013.08.002.
[40] R. Maio, T.M. Ferreira, J.M.C. Estêvão, B. Pantò, I. Caliò, R. Vicente, Seismic performance-based assessment of urban cultural heritage assets through different macroelement approaches, J. Build. Eng. 29 (2020), 101083, https://doi.org/10.1016/j.jobe.2019.101083.
[41] M. Tomazevic, The Computer Program POR: Institute for Testing and Research in Materials and Structures-ZRMK, 1978. Slovenia: Ljubljana.
[42] J.K. Shrestha, S. Bhandari, S. Pradhan, D. Gautam, Simplified frame model for capacity assessment of masonry buildings, Soil Dynam. Earthq. Eng. 131 (2020), https://doi.org/10.1016/j.soildyn.2020.106056, 106056.
[43] A. Penna, S. Lagomarsino, A. Galasco, A nonlinear macroelement model for the seismic analysis of masonry buildings, Earthq. Eng. Struct. Dynam. 43 (2014) 159–179, https://doi.org/10.1002/eqe.2335.
[44] S. Bracchi, A. Galasco, A. Penna, A Novel Macroelement Model for the Nonlinear Analysis of Masonry Buildings. Part 1: Axial and Flexural Behavior, Earthquake Engineering & Structural Dynamics, 2021, https://doi.org/10.1002/eqe.3445.
[45] S. Bracchi, A. Penna, A Novel Macroelement Model for the Nonlinear Analysis of Masonry Buildings. Part 2: Shear Behavior, Earthquake Engineering & Structural Dynamics, 2021, https://doi.org/10.1002/eqe.3444.
[46] R. Siano, P. Roca, G. Camata, L. Pelà, V. Sepe, E. Spacone, et al., Numerical investigation of non-linear equivalent-frame models for regular masonry walls, Eng. Struct. 173 (2018) 512–529, https://doi.org/10.1016/j.engstruct.2018.07.006.
[47] M. Peruch, E. Spacone, G. Camata, Nonlinear analysis of masonry structures using fiber-section line elements, Earthq. Eng. Struct. Dynam. 48 (2019) 1345–1364, https://doi.org/10.1002/eqe.3188.
[48] H. Xu, C. Gentilini, Z. Yu, H. Wu, S. Zhao, A unified model for the seismic analysis of brick masonry structures, Construct. Build. Mater. 184 (2018) 733–751, https://doi.org/10.1016/j.conbuildmat.2018.06.208.
[49] J. Park, P. Towashiraporn, J.I. Craig, B.J. Goodno, Seismic fragility analysis of low-rise unreinforced masonry structures, Eng. Struct. 31 (2009) 125–137, https://doi.org/10.1016/j.engstruct.2008.07.021.

[50] G. Rinaldin, C. Amadio, L. Macorini, A macro-model with nonlinear springs for seismic analysis of URM buildings, Earthq. Eng. Struct. Dynam. 45 (2016) 2261–2281, https://doi.org/10.1002/eqe.2759.
[51] K. Orakcal, J.W. Wallace, J.P. Conte, Flexural modeling of reinforced concrete walls-model attributes, Struct. J. 101 (2004) 688–698.
[52] K. Orakcal, J.W. Wallace, Flexural modeling of reinforced concrete walls-experimental verification, ACI Mater. J. 103 (2006) 196.
[53] S. Mazzoni, F. McKenna, M.H. Scott, G.L. Fenves, OpenSees Command Language Manual. Pacific Earthquake Engineering Research (PEER) Center, 2006, p. 264.
[54] K. Kolozvari, K. Orakcal, J.W. Wallace, Modeling of cyclic shear-flexure interaction in reinforced concrete structural walls. I: Theory, J. Struct. Eng. 141 (2015), 04014135, https://doi.org/10.1061/(ASCE)ST.1943-541X.0001059.
[55] K. Kolozvari, T.A. Tran, K. Orakcal, J.W. Wallace, Modeling of cyclic shear-flexure interaction in reinforced concrete structural walls. II: experimental validation, J. Struct. Eng. 141 (2015), 04014136, https://doi.org/10.1061/(ASCE)ST.1943-541X.0001083.
[56] K. Kolozvari, K. Orakcal, J.W. Wallace, New opensees models for simulating nonlinear flexural and coupled shear-flexural behavior of RC walls and columns, Comput. Struct. 196 (2018) 246–262, https://doi.org/10.1016/j.compstruc.2017.10.010.
[57] J. Park, Investigation of the geometric variation effect on seismic performance of low-rise unreinforced masonry structures through fragility analysis, Int. J. Civ. Eng. 16 (2018) 93–106, https://doi.org/10.1007/s40999-016-0070-x.
[58] J. Craig, B. Goodno, P. Towashiraporn, J. Park, Response Modification Applications for Essential Facilities, Project ST-4 Final Report, Georgia Institute of Technology, The United States, 2007.
[59] A. Shabani, V. Plevris, M. Kioumarsi, A Comparative Study on the Initial In-Plane Stiffness of Masonry Walls with Openings. 17th World Conference on Earthquake Engineering, 17WCEE. Sendai, Japan, 2021.
[60] K. Demirlioglu, S. Gonen, S. Soyoz, M.P. Limongelli, In-plane seismic response analyses of a historical brick masonry building using equivalent frame and 3D FEM modeling approaches, Int. J. Architect. Herit. (2018), https://doi.org/10.1080/15583058.2018.1529208.
[61] M. Dolce, Schematizzazione e modellazione degli edifici in muratura soggetti ad azioni sismiche, L'industr. Costr. 25 (1991) 44–57 (in Italian).
[62] G. Magenes, G. Kingsley, G. Calvi, Seismic Testing of a Full-Scale, Two-Story Masonry Building: Test Procedure and Measured Experimental Response Report 3.0, G.N.D.T. Department of Structural Mechanics, University of Pavia, 1995.
[63] P. Esmaeiltabar, J. Vaseghi, H. Khosravi, Nonlinear macro modeling of slender reinforced concrete shear walls, Struct. Concr. 20 (2019) 899–910, https://doi.org/10.1002/suco.201800206.
[64] G. Rinaldin, C. Amadio, N. Gattesco, Review of experimental cyclic tests on unreinforced and strengthened masonry spandrels and numerical modelling of their cyclic behaviour, Eng. Struct. 132 (2017) 609–623, https://doi.org/10.1016/j.engstruct.2016.11.063.
[65] S. Cattari, S. Lagomarsino, A strength criterion for the flexural behaviour of spandrels in un-reinforced masonry walls, in: The 14th World Conference on Earthquake Engineering. Beijing, China, 2008.
[66] A. Anthoine, G. Magonette, G. Magenes, Shear-compression testing and analysis of brick masonry walls, Tenth Eur. Conf. Earthq. Eng. 3 (1995) 1657–1662.
[67] G.M.A. Schreppers, A. Garofano, F. Messali, J.G. Rots, DIANA Validation Report for Masonry Modelling, DIANA FEA Report 2016-DIANA-R1601, Delft University of Technology, Netherland, 2016, p. 143.
[68] K. Kolozvari, J.W. Wallace, Practical nonlinear modeling of reinforced concrete structural walls, J. Struct. Eng. 142 (2016), G4016001, https://doi.org/10.1061/(ASCE)ST.1943-541X.0001492.
[69] S. Cattari, D. Camilletti, A.M. D'Altri, S. Lagomarsino, On the use of continuum Finite Element and Equivalent Frame models for the seismic assessment of masonry walls, J. Build. Eng. 43 (2021), 102519, https://doi.org/10.1016/j.jobe.2021.102519.
[70] N. Gattesco, L. Macorini, A. Dudine, Experimental response of brick-masonry spandrels under in-plane cyclic loading, J. Struct. Eng. 142 (2016), 04015146, https://doi.org/10.1061/(ASCE)ST.1943-541X.0001418.
[71] D. Vamvatsikos, C.A. Cornell, Incremental dynamic analysis, Earthq. Eng. Struct. Dynam. 31 (2002) 491–514, https://doi.org/10.1002/eqe.141.
[72] D. Vamvatsikos, C.A. Cornell, Applied incremental dynamic analysis, Earthq. Spectra 20 (2004) 523–553, https://doi.org/10.1193/1.1737737.
[73] N. Mohammadgholibeyki, M. Banazadeh, The effects of viscous damping modeling methods on seismic performance of RC moment frames using different nonlinear formulations, Structures 15 (2018) 232–243, https://doi.org/10.1016/j.istruc.2018.07.009.
[74] FEMA, Quantification of Building Seismic Performance Factors, FEMA P695, Federal Emergency Management Agency, United States, Washington, D.C., 2009.
[75] A. Zaherdannak, A. Shabani, S. Erfani, Seismic performance evaluation of special RC frames with gravity steel columns under the base level, Shock Vib. (2020), https://doi.org/10.1155/2020/8825258, 2020:8825258.
[76] V.G. Haach, G. Vasconcelos, P.B. Lourenço, Parametrical study of masonry walls subjected to in-plane loading through numerical modeling, Eng. Struct. 33 (2011) 1377–1389, https://doi.org/10.1016/j.engstruct.2011.01.015.